Journal of Applied Electrochemistry (2018) 48:243–250
https://doi.org/10.1007/s10800-018-1154-x

RESEARCH ARTICLE

An aluminium battery operating with an aqueous electrolyte

A. Holland[1] · R. D. Mckerracher[1] · A. Cruden[1] · R. G. A. Wills[1]

Received: 4 August 2017 / Accepted: 17 January 2018 / Published online: 2 February 2018

Abstract

Aluminium is an attractive active material for battery systems due to its abundance, low cost, a gravimetric energy density of 2.98 Ah g^{-1} (c.f. lithium 3.86 Ah g^{-1}) and a volumetric energy density of 8.04 Ah cm^{-3} (c.f. lithium 2.06 Ah cm^{-3}). An aqueous electrolyte-based aluminium-ion cell is described using TiO_2 nanopowder as the negative electrode, CuHCF (copper-hexacyanoferrate) as the positive electrode and an electrolyte consisting of 1 mol dm^{-3} $AlCl_3$ and 1 mol dm^{-3} KCl. Voltammetric and galvanostatic analyses have shown that the discharge voltage is circa 1.5 V. Both a single-cell and 2-cell battery are demonstrated using 10 cm^2 electrodes and 126 and 256 mg total active material for the 1-cell and 2-cell batteries, respectively. The single cell exhibits an energy density of circa 15 mW h g^{-1} (combined positive and negative electrode masses) at a power density of 300 mW g^{-1} with energy efficiency remaining above 70% for over 1750 cycles. Initial characterisation shows that charge storage is due to the presence of Al^{3+}. Cell capacity is circa 10 mA h g^{-1} and operates with a discharge voltage of circa 1.5 V (efficiency > 80% at 20C charge/discharge rate).

Graphical Abstract

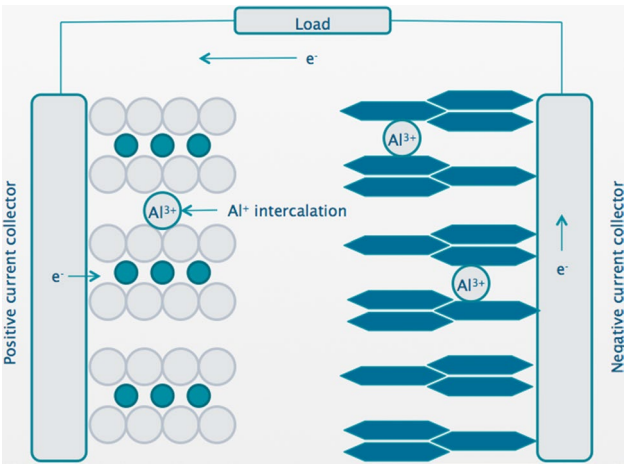

Keyword Aqueous aluminium ion battery

1 Introduction

The consumption of renewable energy, excluding hydropower, has grown almost exponentially over the past 20 years [1]. Most of this growth has come in the form of distributed solar PV and wind power which can cause a number of problems for electricity grids. For example, cloud cover can cause output from solar PV plants to be subject to

✉ R. G. A. Wills
rgaw@soton.ac.uk

[1] Faculty of Engineering and the Environment, University of Southampton, Highfield, Southampton SO17 1BJ, UK

large voltage and power fluctuations. This can be alleviated through use of low energy but high power, high cycle life and fast response energy storage systems [2]. Given suitable electrode materials, the high conductivity of aqueous electrolytes mean aqueous intercalation batteries may be capable of providing these characteristics in addition to being safe, non-toxic and potentially low-cost when compared to non-aqueous systems, such as ionic liquids. This communication reports on the construction and testing of a fully functional aqueous Al-ion cell. It should be noted that the majority of Al-ion research focusses on room temperature ionic liquid electrolyte systems (RTILs) theoretically allowing the utilisation of aluminium metals high capacity through reversible deposition [3–10]. The primary research aim becomes the identification of positive electrode materials that will not severely limit cell capacity. Table 1 provides an overview of RTIL-based Al-ion systems reported in the literature to date. Cycle life varies from just 50 to 7500. Applied currents also vary considerable between reported electrodes, from 12 up to 5000 mA g^{-1}. The majority of studies use $AlCl_3$/EMICl (1-ethyl-3-methylimidazolium chloride) or $AlCl_3$/BMICl (1-butyl-3-methylimidazolium chloride) as the electrolyte. Given a suitable positive electrode, a high capacity and energy density cell could be constructed. The best-performing cell to date, with a natural graphite positive electrode, has achieved a capacity of c.a. 100 mA h g^{-1} when cycled at 198 mA g^{-1}. However, the expense and corrosiveness of RTILs are significant disadvantages of such a battery system.

The use of water as solvent for an aluminium salt has the potential to provide a cheap, inherently safe and more conductive electrolyte system compared to RTILs. Table 2 summarises the literature available for the aqueous aluminium ion battery. Only three electrode materials, anatase TiO_2, copper-hexacyanoferrate (CuHCF), and aerogel V_2O_5, have been shown to allow the reversible intercalation of Al^{3+} in aqueous electrolytes [11–16]. The most successful negative electrode was black-anatase TiO_2, reported by He et al. [11] that produced a high capacity of 270 mAh g^{-1}, in 1 mol dm^{-3} $Al(NO_3)_3$, although only 300 cycles were reported. CuHCF was shown by Liu et al. to give a capacity of 41 mAh g^{-1} at 400 mA g^{-1} in 0.5 mol dm^{-3} $Al_2(SO_4)_3$ [12]. A capacity fade of 41% was measured over 1000 cycles. CuHCF has also been tested as a positive electrode for an Al-ion cell containing organic electrolyte but reversible capacity was low at 5–14 mA h g^{-1} [13]. However, CuHCF, along with a number of other hexacyanoferrates, has also been shown to function as positive electrodes in other aqueous electrolytes containing K^+, Na^+, Mg^{2+} or Zn^{2+} [14–17]. Specific capacities of approximately 50–60 mA h g^{-1} are often reported. It should be noted that the capacities quoted regarding aqueous Al-ion cells are for individual electrode materials and not operational cells, where the positive and negative materials must be jointly considered. Furthermore, these studies have been limited to half-cell analysis and not operated in a battery configuration. In this paper, we discuss the electrochemical performance of a combined cell and a two-cell battery, demonstrating an operational system based on an aqueous electrolyte containing Al^{3+}.

2 Experimental procedure

Anatase-TiO_2 nanopowder (< 25 nm) was used as received from Sigma Aldrich. Electrode inks were prepared through the addition of TiO_2, carbon black (CB), and Nafion binder, in the ratio 9:0.5:0.5 by wt%. The positive electrode consisted of CuHCF, carbon black (CB), and Nafion binder in the ratio 8:1:1. Propanol was added to form inks of suitable viscosity (approximately 3:1 propanol:active material) and mixed at 5000 rpm for 30 min using Silverson shear blade mixer. The resulting inks were coated onto Sigracell PV10 carbon polymer current collectors from SGL and left to dry in ambient conditions.

CuHCF was prepared through a standard precipitation method. 1.5 mol dm^{-3} solution $Cu(NO_3)_2$ was added to 1 mol dm^{-3} solution of $K_3[Fe(CN)_6]$ and stirred for a minimum of 2 h at room temperature. The precipitate was centrifuged and washed five times before drying in air at 80 °C and grinding to form CuHCF powder.

Standard 3-electrode glass cells were used for cyclic voltammetry (CV) to characterise the electrochemical activity of TiO_2 in aqueous electrolytes. A saturated calomel electrode (SCE) was used as the reference electrode and a platinum wire as the counter electrode. An Ivium multichannel electrochemical analyser was used for CV scans. The galvanostatic performance of both electrodes was investigated in full cells through oversizing of the opposing electrode so that the cell capacity was only dictated by the electrode under investigation. An SCE reference electrode was used, in connection with a National Instruments data acquisition module, for voltage measurements of individual electrodes when being operated in a full cell, see Fig. 1. For these 2-electrode experiments, capacities of 16 and 50 mA h g^{-1} were assumed for TiO_2 and CuHCF, respectively, such that a 20C cycle rate corresponds to 333 mA g^{-1} for TiO_2 and 1000 mA g^{-1} for CuHCF. A balanced cell, where the TiO_2-electrode capacity was approximately equal to CuHCF-electrode capacity, used 10 cm^2 of each active material on carbon polymer, separated by an electrolyte cavity, as shown in Fig. 1. Positive and negative electrode loadings were 3.8 and 8.5 mg cm^{-2} for the final cell, constituting larger format electrodes than previously reported. Electrode loadings for the 2-cell battery were 3.6 and 9.2 mg cm^{-2}. When operated as a unit cell, the positive electrode (CuHCF) acted as the working electrode for the Ivium analyser, with the negative

Table 1 Comparing Al-ion cells utilising room temperature ionic liquid (RTIL) electrolytes

Paper	Electrode and electrolyte	Specific capacity	Cyclability	Coulombic efficiency	Voltage range/profile
D.-Y Wang et al., *Nat Comm 8*, 2017 [3]	Natural graphite/Al. $AlCl_3$/EMICl	~ 60 mAh g^{-1} at 660 mA g^{-1}. 100 mAh g^{-1} at 198 mA g^{-1}	6000 cycles	~ 100%	2 plateaus between 2.5 and 1.5 V
S. Wang et al., *ACS Nano 11*, 2017 [4]	CuS-C composite/Al. $AlCl_3$/EMICl	~ 100 mAh g^{-1} at 20 mA g^{-1}	300 cycles	~ 100%	Charged between 1.3 and 2 V. Limited discharge plateau between 1.05 and 0.1 V
Angell et al., *PNAS 114*, 2016 [5]	Graphite/Al metal. $AlCl_3$/urea	~ 73 mAh g^{-1} at 100 mA g^{-1}	180 cycles	100 – 99%	2 plateaus between 2.2 and 1.0 V
Lin et al., *Nature 520*, 2015 [6]	Graphitic foam/Al metal. $AlCl_3$/EMICl	~ 60 mAh g^{-1} at 5000 mA g^{-1}	7500 cycles	> 95%	Plateau between 2.5 and 1.5 V
	Pyrolytic graphite/Al metal. $AlCl_3$/EMICl	~ 65 mAh g^{-1} at 66 mA g^{-1}	Stable over 200 cycles	~ 98%	Plateau between 2.25 and 2.0 V
Sun et al., *Chem. Comms 51*, 2015 [7]	Carbon paper/Al foil. Molybdenum current collector. $AlCl_3$/EMICl	~ 70 mAh g^{-1} at 100 mA g^{-1}	Good capacity retention over 100 cycles—graphite layer spacing increases by ~ 38%	~ 100% after 3rd cycle	Plateau between 1.8 and 1.4 V under discharge
Wang et al., *App. Mater. Interfaces 7*, 2015 [8]	V_2O_5 (binder free)/Al metal. $AlCl_3$/EMICl	239 mAh g^{-1} at 44.2 mA g^{-1}	Decreases to ~ 180 mAh g^{-1} after 5th cycle	–	Limited plateau between 0.7 and 0.5 V
Geng et al., *Chem. Mater. 27*, 2015 [9]	Mo_6S_8/Al metal. $AlCl_3$/BMICl	70 mAh g^{-1} at 12 mA g^{-1}. 40 mAh g^{-1} at 60 mA g^{-1}	Stable from 3rd to 50th cycles	> 100%	Two plateaus. Dominant plateau between 0.55 and 0.5 V
Hudak, *J. Phys. Chem. 118*, 2014 [10]	Conducting polymers/Al metal. $AlCl_3$/EMICl	70–45 mAh g^{-1} at 20 mA g^{-1} (polypyrrole) 90–70 mAh g^{-1} at 16 mA g^{-1} (polythiophene)	15% fade up to 100 cycles. Negligible fade from 50th to 400th	> 91% columbic (polypyrrole), > 96% (polythiophene)	0.6–1.9 V/no plateaus

Table 2 Comparing electrodes used in aqueous aluminium electrolytes

Paper	Electrode and electrolyte	Specific capacity	Cyclability	Columbic efficiency[a]	Voltage range/profile
Kazazi et al., *Solid state Ionics 300*, 2017 [18]	Half-cell—TiO_2 nano-spheres. 1 M $AlCl_3$. (0.785 cm^2)	180 mAh g^{-1} at 50.25 mA g^{-1}. 105 mAh g^{-1} at 2010 mA g^{-1}	~6% fade over 30 cycles	~90% from 50.25 mA g^{-1} 2010 mA g^{-1}	− 0.3–1.2 V vs. Ag/AgCl. discharge plateau at − 0.95–0.9 V
Gonzalez et al., *RSC Advances 6*, 2015 [19]	Half-cell—V_2O_5 aerogel. 1 M $AlCl_3$. (Swagelok-T)	120 mAh g^{-1} at 60 mA g^{-1}. ~15 mAh g^{-1} at 200 mA g^{-1}	~40% fade at 60 mA g^{-1} and ~25% fade at 200 mA g^{-1} over 13 cycles	~85%	− 0.4–0.15 V vs. MSE. discharge plateau at − 0.15 V
Liu et al., *J. Mater. Chem. 3*, 2015 [12]	Half-cell—CuHCF. 0.5 M $Al_2(SO_4)_3$. (<2 mg, 0.5 cm^2)	41 mAh g^{-1} at 400 mA g^{-1}	45% fade over 1000 cycles	~100%	1–0.2 V. No plateau
He et al., *J. Mater. Chem. 2*, 2014 [11]	Half-cell—TiO_2 nano-leaves. 1 M $Al(NO_3)_3$. (9 mg)	271 mAh g^{-1} at 50 mA g^{-1}. 141 mAh g^{-1} at 2 A g^{-1}	8.4% fade after 300 cycles at 50 mA/g	~100%	1.35–0.45 V. discharge plateau at ~0.97 V[b]
Y. Liu et al., *Electro. Acta 143*, 2014 [20]	Half-cell—TiO_2 nano-wire array. 0.5 M $Al_2(SO_4)_3$	75 mAh/g at 4 mA/cm^2	–	~85%	1.1–0.9 V/discharge plateau just below 1 V
Liu et al., *Energy and Environ. Science 5*, 2012 [21]	Half-cell. TiO_2 nano-tube array film. 1 M $AlCl_3$	75 mAh g^{-1} at 4 mA cm^{-2}	–	~90%	1.1–0.4 V/discharge plateau between 1.1 and ~0.8 V

[a]Some coulombic efficiencies had to be estimated from charge/discharge cycles and assumed constant and accurate current densities as described

[b]From the charge–discharge cycle, of TiO_2/Al cell, presented in the papers supplementary material

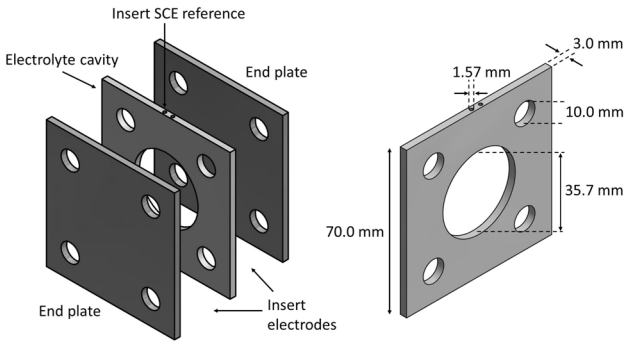

Fig. 1 Schematic of the cell configuration used for the aqueous Al-ion cell. End plates were made of stainless steel and electrolyte cavity insert of PEEK

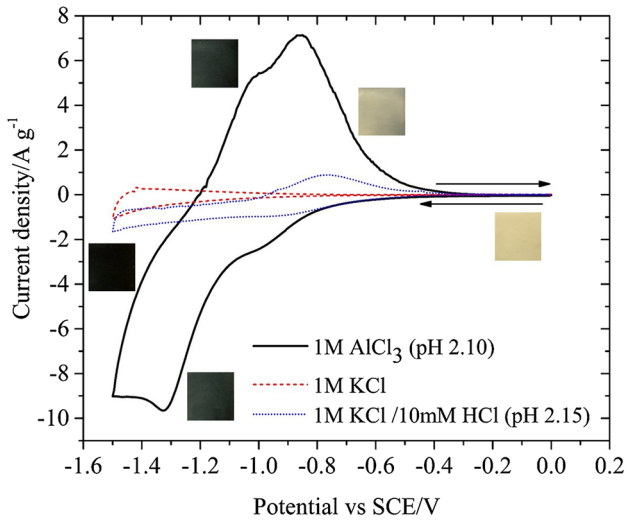

Fig. 2 Cyclic voltammetry of a TiO_2 electrode in 1 mol dm^{-3} $AlCl_3$ as well as 'blank' electrolytes consisting of 1 mol dm^{-3} KCl and 1 mol dm^{-3} KCl with 10 mmol dm^{-3} HCl. A scan rate of 10 mV s^{-1} was used

electrode (TiO_2) being connected to the counter and reference electrode terminals.

Neutron diffraction analysis was obtained using the GEM diffractometer via GEM Xpress operated at ISIS under project numbers (RN 1690193 and 1690194). Data sets were interpreted by the facility.

3 Results and discussion

A cyclic voltammogram was obtained at a TiO_2 electrode (cell anode) in aqueous 1 mol dm^{-3} $AlCl_3$, 1 mol dm^{-3} KCl, and 1 mol dm^{-3} KCl/10 mmol dm^{-3} HCl. The potential was swept from 0 to − 1.5 V vs. SCE before returning to 0 V. A constant sweep rate of 10 mV s^{-1} was maintained

throughout. Figure 2 presents the voltammogram with overlaying photographic images of the electrode surface at key potentials. Towards negative potentials, a reduction wave associated with Al^{3+} interacting with the TiO_2 electrode commences at circa −0.8 V with an associated peak at circa −1.31 V. The current peaks at −9.7 A g^{-1}. On the reverse sweep, an oxidation wave is observed, with a peak of 7.2 A g^{-1}, at −0.85 V. Both reduction and oxidation waves have secondary peaks, at circa 0.98 V and circa −1.05 V respectively, indicating more than one reaction process associated with the TiO_2/Al^{3+} interaction. In 1 mol dm^{-3} $AlCl_3$, electrolyte stability at the electrode is good, with the onset of H_2 evolution not yet visible at −1.5 V. An electrolyte containing 1 mol dm^{-3} KCl gave rise to no discernible redox activity, however, demonstrating that the redox phenomena are linked to the presence of Al^{3+} in the electrolyte solution. With the addition of HCl, small reduction and oxidation peaks, of approximately 1 A g^{-1}, became apparent at roughly −0.9 and −0.8 V, respectively. This suggests an inherent response from anatase TiO_2 in acidic aqueous electrolyte, which is an order of magnitude smaller in capacity than the response obtained in the presence of Al^{3+}.

Photographic images were periodically taken, during a scan of a TiO_2-only electrode, and have been overlaid at the appropriate potentials in Fig. 2. These images graphically show the charge/discharge process at the negative electrode. In the charged state, the electrode is dark blue-grey, while in the discharged state the electrode almost returns to the original white colour associated with TiO_2. These changes could be attributed to the reduction of Ti^{4+} to Ti^{3+} via four possible processes: Al^{3+} surface adsorption, Al^{3+} intercalation, H^+ surface adsorption and/or H^+ intercalation. Further mechanistic studies are planned to fully elucidate the processes involved.

The effect of acidity on the response is shown in Fig. 3. Anodic peak currents are seen to decrease with increasing acidity, while cathodic peaks became decreasingly prominent, due to hydrogen evolution. This suggests that increasing the acidity of the electrolyte would be detrimental to cell performance. In conjunction with Fig. 1, it can be concluded that the redox activity of anatase TiO_2 is primarily due to the presence of Al^{3+} and not protons.

Neutron diffraction analysis of the negative electrode was carried out at ISIS using the General Materials Diffractometer (GEM). Two runs were undertaken: 79453 (freshly prepared electrode) and 79454 (electrode after charge/discharge cycling). The results showed a very good fit to a TiO_2 structure with the two data sets having the following lattice parameters: 79453 a @ 3.7707(9), b @ 3.7706(10), c @ 9.4631(23), and 79454 a @ 3.7697(9), b @ 3.7695(10), c @ 9.4589(24). That is a difference of 0.001 Angstroms in a, 0.002 in b and 0.004 in c. This is a very slight shift in lattice parameters between an unused electrode and one that has been exposed to Al^{3+} in a battery environment. This represents a shift higher than the measured error (by an order of magnitude in a, by a factor of 2 in b and c) and so may be significant. While this lattice expansion may be evidence of Al^{3+} intercalation, further analysis is required on in situ electrodes over a range of states of charge to validate the mechanism.

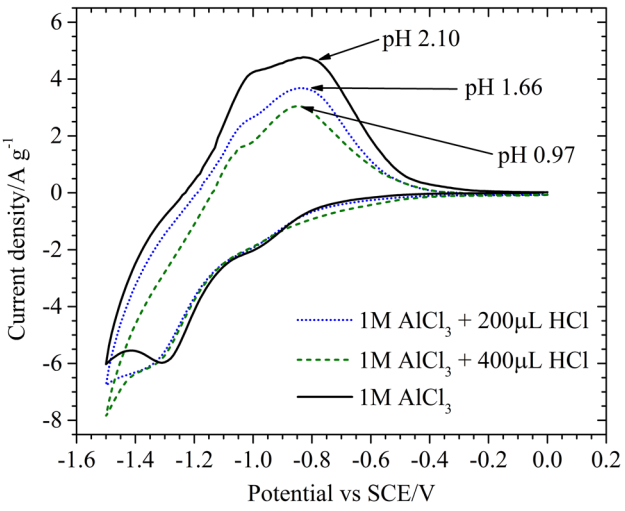

Fig. 3 Cyclic voltammetry of a TiO_2 electrode in 1 mol dm^{-3} $AlCl_3$ electrolytes of increasing acidity. A scan rate of 10 mV s^{-1} was used

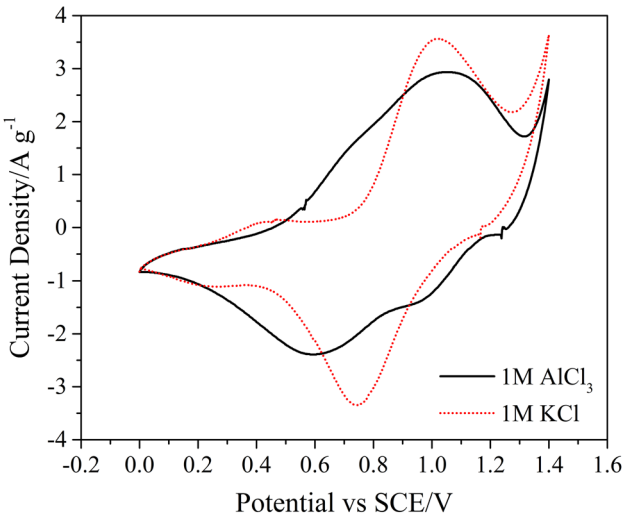

Fig. 4 Cyclic voltammetry of CuHCF at 20 mV s^{-1} in 1 mol dm^{-3} $AlCl_3$ and 1 mol dm^{-3} KCl. An SCE and Pt-wire were used as reference and counter electrodes

Cyclic voltammograms were obtained at CuHCF electrodes (cell cathode) in 1 mol dm^{-3} $AlCl_3$ and 1 mol dm^{-3} KCl. The voltammetric response is presented in Fig. 4. In 1 mol dm^{-3} $AlCl_3$, broad reduction and oxidation peaks are visible at 0.6 and 1.05 V, respectively. Broad shoulders are

also observed during the anodic and cathodic sweeps, centred on 0.7 and 1.0 V, respectively. Bulk oxygen evolution was observed at potentials more positive than 1.3 V vs. SCE. 1 mol dm^{-3} KCl produces sharper peaks at 0.74 and 1.0 V, suggesting more facile insertion of K^+ than Al^{3+}. The use of a mixed Al^{3+}/K^+ electrolyte may therefore provide favourable cell operation where TiO_2 and CuHCF are utilised as the negative and positive electrodes.

With redox activity of TiO_2 and CuHCF in Al^{3+} containing electrolyte confirmed, the performance of these electrodes was tested in aqueous Al-ion cells. Cells were limited by a single electrode by ensuring the capacity of the opposite electrode was considerably larger. TiO_2 was galvanostatically charged to a specific capacity at a current density of 333 mA g^{-1}. Figure 5 shows the discharge capacity and coulombic efficiency of TiO_2 as a function of charge input. Above a 16–17 mA h g^{-1} charge input, there is limited increase in discharge capacity while the associated coulombic efficiency drops dramatically from > 80% to < 50% at beyond 30 mAh g^{-1}. Both TiO_2- and CuHCF-limited 2-electrode cells were then cycled at a charge and discharge current density of 333 mA g^{-1} for 1000 cycles. The results are summarised in Table 3. TiO_2 produced a capacity of 14.5 mA h g^{-1} which decreased by ~ 7% after 1000 cycles (c.f. 45% capacity fade over 1000 cycles previously reported in the literature [13]) demonstrating that while the capacity is initially low, the electrode material and architecture are robust. The TiO_2 electrode was cycled. The capacity is considerably lower than would be expected from an intercalation electrode. The theoretical capacity of TiO_2 is 335 mA h g^{-1} assuming intercalation proceeds according to reaction 1 [11], where $0 < x < 1/3$since charge capacity is likely limited by the Ti^{4+}/Ti^{3+} couple. This suggests

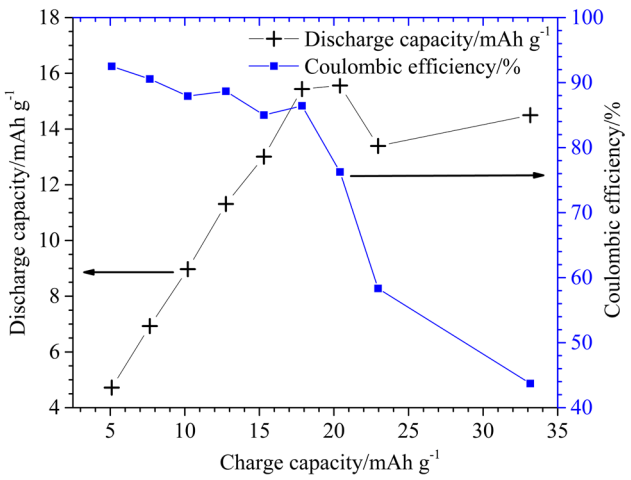

Fig. 5 The discharge capacity and coulombic efficiency of a TiO_2 electrode as a function of charge capacity when cycled at 333 mA g^{-1} in 1 mol dm^{-3} $AlCl_3$/1 mol dm^{-3} KCl

Table 3 Summary of performance of TiO_2- and CuHCF- limited cells cycled in 1 mol dm^{-3} $AlCl_3$ and 1 mol dm^{-3} KCl at a current density of 333 mA g^{-1} (based on the mass of the limiting electrode)

	TiO_2 (333 mA g^{-1})	CuHCF (1000 mA g^{-1})
Capacity	14 mA h g^{-1}	50 mA h g^{-1}
Average discharge voltage	− 0.65 V vs. SCE	0.70 V vs. SCE
Coulombic efficiency	84 – 80%	92–94%
Energy efficiency	72 – 66%	66%
Cycled to	> 1000	> 1000

Al^{3+} surface adsorption to be the most likely charge storage mechanism.

$$TiO_2 + xAl^{3+} + 3xe^- \leftrightarrow Al_xTiO_2 \quad (1)$$

The coulombic efficiency of TiO_2 remained around 80% while the energy efficiency decreased by only 5% from a maximum of 71%. The more negative voltage profile in Fig. 6 corresponds to the TiO_2 electrode, vs. SCE, during cycling. A very small initial voltage hysteresis shows that the electrode should be capable of discharge at higher rates; however, coulombic efficiency is clearly low and may be indicative of a simultaneous self-discharge process.

Galvanostatic cycling of CuHCF at 1000 mA g^{-1} produced a capacity of ~ 50 mAh g^{-1} throughout > 1000 cycles. Coulombic efficiency was 97.2% after 20 cycles and decreased to 94%; energy efficiency of the CuHCF-limited cell remained at ~ 66% over > 1000 cycles, which surpasses the previously reported cycling of electrodes incorporating

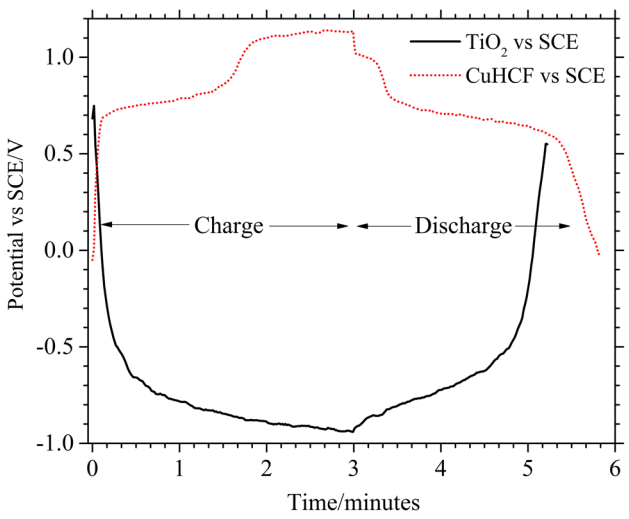

Fig. 6 Top (red-dotted): typical voltage profile, vs. SCE, of a CuHCF electrode under cycling at 1000 mA g^{-1}. Bottom (black-solid): typical voltage profile, vs. SCE, of a TiO_2 electrode under cycling at 333 mA g^{-1}. A 1 mol dm^{-3} $AlCl_3$/1 mol dm^{-3} KCl electrolyte was used in both cells. (Color figure online)

CuHCF [5]. The more positive voltage profile in Fig. 6 corresponds to CuHCF during a typical cycle. During charge, two plateaus are visible at 0.75 and 1.1 V, each accounting for approximately half of the charge capacity. Similarly, two discharge plateaus are visible at 0.98 and 0.65 V, although the first discharge plateau accounts for only 7% of the discharge capacity. The nature of the two plateaus is not yet understood. The 0.1 V hysteresis between final charge voltage and initial discharge voltage suggests that the rate capability of CuHCF may be inferior to TiO_2, although coulombic efficiency is clearly superior. The < 100% efficiency is attributed to side reactions such as O_2 evolution.

A balanced cell (85 mg TiO_2 vs. 38 mg CuHCF) was cycled nearly 2000 times at a current corresponding to a 20C rate. The efficiencies and discharge capacity throughout cycling are shown in Fig. 7 with the evolution of the voltage profile given in Fig. 8. A maximum capacity, calculated from the combined mass of electrodes, of circa 10.6 mA h g^{-1} remained above 10 mA h g^{-1} until the 1814th cycle. An average discharge voltage which ranged between 1.49 V at cycle 100 and 1.46 V at cycle 1750 gives the cell an energy density of ca. 15 mW h g^{-1}. An initial coulombic efficiency of 96% was still above 90% by the 1900th cycle; energy efficiency decreased from ~80 to 70% at cycle number 1778. Therefore, while capacity and energy density remain low, a cell with good voltage, cycle life, efficiency and rate capability has been demonstrated.

A 2-cell aqueous Al-ion battery is also demonstrated using a bipolar electrode. The voltage vs. time profile is compared to a single cell in Fig. 9. The charge and voltage efficiencies are comparable. Cycling at a 10C rate, the charge voltage increases steadily from circa 2.0 to 3.5 V, at which point there is a more rapid increase in voltage to 4.1 V before a further steady increase to 4.5 V at the end of charge. During discharge, the voltage decreases steadily from 4.0 to 3.7 V, at which point there is a rapid drop-off to 3.4 V followed by a more steady decline to 2.0 V at the end of discharge. From Fig. 5, the two-voltage stages are associated with the CuHCF positive electrode. An average discharge voltage of 2.93 V was achieved, giving the battery an energy density of 14.8 mW h g^{-1} according to total mass of active material in both electrodes.

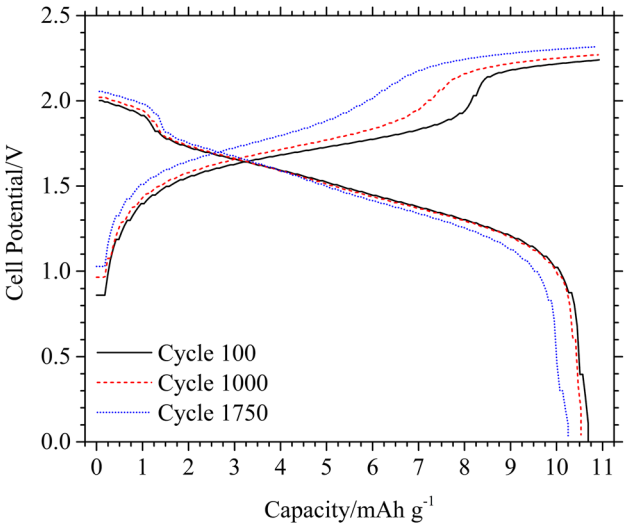

Fig. 8 Evolution of the charge/discharge profile of the aqueous Al-ion cell under extended cycling at 20C in 1 mol dm^{-3} $AlCl_3$/1 mol dm^{-3} KCl

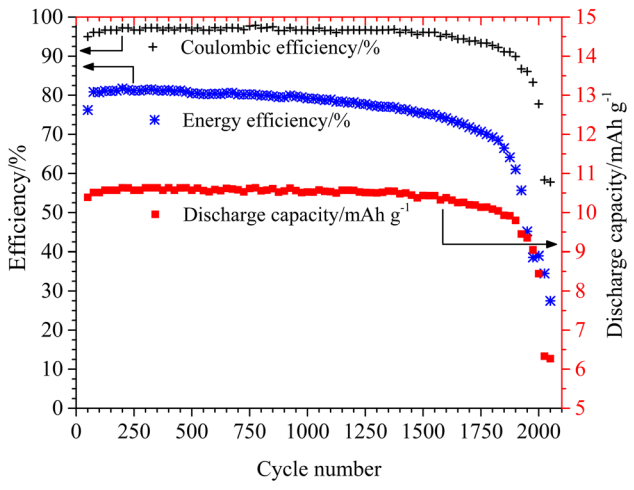

Fig. 7 Performance of a balanced Al-ion cell consisting of TiO_2 negative electrode, CuHCF positive electrode and 1 mol dm^{-3} $AlCl_3$/mol dm^{-3} KCl electrolyte. A 20C charge/discharge rate was used

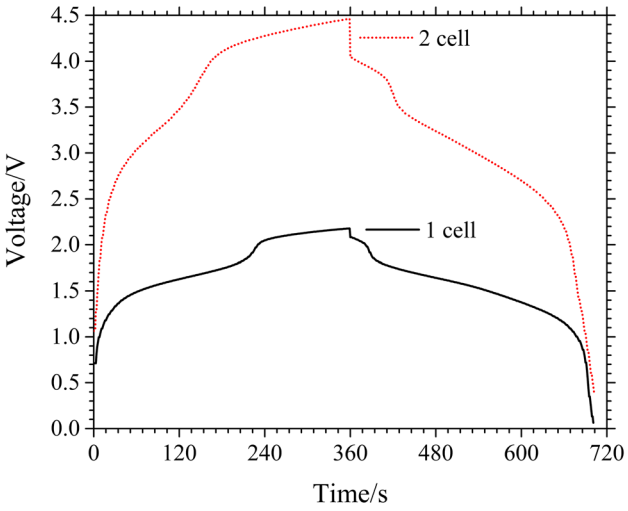

Fig. 9 Typical profile of a 1-cell and 2-cell Al-ion battery cycled at a 10C charge/discharge rate in 1 mol dm^{-3} $AlCl_3$/1 mol dm^{-3} KCl electrolyte

4 Conclusion

The first multi-cell battery based on aqueous aluminium ion chemistry is described. The battery is based on anatase (TiO_2) nanopowder, CuHCF and aqueous Al^{3+}/K^+ electrolyte, which are all widely available, cheap and non-toxic materials, providing advantages over current Li-ion and Pb-acid systems. Although the specific energy is relatively low, ca. 15 mWh g^{-1} active material (combined positive and negative materials), a high charge and discharge rate of 20C is achievable. At the 20 C rate, the energy efficiency of the cell remained above 70% for over 1750 cycles, with only a 7% capacity fade, demonstrating the longevity of the cell. The low specific energy is caused by the TiO_2 anode; the capacity of CuHCF is c.a. 50 mAh g^{-1} at a current density of 333 mA g^{-1}.

The charge storage capacity of TiO_2 was shown to be due to the presence of Al^{3+} rather than the H^+ present in the acidic electrolyte. However, the slight shift in neutron diffraction parameters is not sufficient to ascertain whether the main mechanism of charge storage is via Al^{3+} intercalation or a surface adsorption reaction. Further work on elucidating the mechanism could allow the cell capacity to be increased and the active materials to be tailored, for example towards high surface area materials for a surface process or doped materials for intercalation. Self-discharge exhibited by the TiO_2 electrode, most likely due to the presence of dissolved oxygen, needs to be minimised and investigated further.

Acknowledgements This project has received funding from the European Union's Horizon 2020 research and innovation programme under rant agreement No. 646286. The authors would also like to thank Martin-Owen Jones at STFC for his assistance in interpreting the GEM neutron diffraction data obtained at ISIS.

References

1. BP (2015) BP statistical review of world energy 2015
2. EPRI (2010) Electricity energy storage options: a white paper on applications, costs and benefits. EPRI, Palo Alto
3. Wang. D-Y et al (2017) Advanced rechargeable aluminium ion battery with a high-quality natural graphite cathode. Nat Commun 8:14283
4. Wang S et al (2017) High-performance aluminum-ion battery with CuS@C microsphere composite cathode. ACS Nano 11:469–477
5. Angell M, Pan C-J, Rong Y, Yuan C, Lin M-C, Hwang B-J, Dai H (2016) High Coulombic efficiency aluminum-ion battery using an AlCl3-urea ionic liquid analog electrolyte. PNAS 114, 5:834–839
6. Lin M-C, Gong M, Lu B, YingpengWu D-Y, Wang M, Guan M, Angell C, Chen J, Yang B-J, Hwang H, Dai (2015) An ultrafast rechargeable aluminium-ion battery. Nature 520:325–328
7. Sun H, Wang W, Yu Z, Yuan Y, Wang S, Jiao S (2015) A new aluminium-ion battery with high voltage, high safety and low cost. Chem Commun 51:11892–11895
8. Wang H, Bai Y, Chen S, Luo X, Wu C, Wu F, Lu J (2015) Binder-free V_2O_5 cathode for greener rechargeable aluminum battery. Appl Matter Interfaces 7:80–84
9. Geng L, Lv G, Guo XX,J (2015) Reversible electrochemical intercalation of aluminum in Mo6S8. Chem Mater 27:4926–4929
10. Hudak N (2014) Chloroaluminate-doped conducting polymers as positive electrodes in rechargeable aluminum batteries. J Phys Chem 118:5203–5215
11. He YJ, Peng JF, Chu W, Li YZ, Tong DG (2014) Black mesoporous anatase TiO_2 nanoleaves: a high capacity and high rate anode for aqueous Al-ion batteries. J Mater Chem A 2:1721–1731
12. Liu S, Pan GL, Li GR, Gao XP (2015) Copper hexacyanoferrate nanoparticles as cathode material for aqueous Al-ion batteries. J Mater Chem 3:959–962
13. Reed LD, Ortiz SN, Xiong M, Menke EJ (2015) A rechargeable aluminum-ion battery utilizing a copper hexacyanoferrate cathode in an organic electrolyte. Chem Commun 51:14397–14400
14. Pasta M, Wessells CD, Liu N, Nelson J, McDowell MT, Huggins RA, Toney MF, Cui Y (2015) Full open-framework batteries for stationary energy storage. Nat Commun. https://doi.org/10.1038/ncomms4007
15. Trócoli DR, La Mantia DF (2015) An aqueous zinc-ion battery based on copper hexacyanoferrate. ChemSusChem 8:481–485
16. Jia Z, Wang B, Wang Y (2015) Copper hexacyanoferrate with a well-defined open framework as a positive electrode for aqueous zinc ion batteries. Mater Chem Phys 149–150:601–606
17. Wessells CD, Peddada SV, McDowell MT (2012) The effect of insertion species on nanostructured open. J Electrochem Soc 159(2):98–103
18. Kazazi M, Abdollahi P, Mirzaei-Moghadam M (2017) High surface area TiO_2 nanospheres as a high-rate anode material for aqueous aluminium-ion batteries. Solid State Ionics 300:32–27
19. Gonz´alez JR, Nacimiento MCF, Alc´antar R, Lavel P, Tirado aJL (2016) Reversible intercalation of aluminium into vanadium pentoxide xerogel for aqueous rechargeable batteries. RSC Adv 6:62157–62164
20. Liu Y, Wu SSQ, Lu Z, Liu K, Liu H (2014) The electrochemical behavior of Cl^- assisted Al^{3+} insertion intotitanium dioxide nanotube arrays in aqueous solution for aluminumion batteries. Electrochim Acta 143:340–346
21. Liu S, Hu JJ, Yan NF, Pan GL, Li GR, Gao XP (2012) Aluminum storage behavior of anatase TiO_2 nanotube arrays in aqueous solution for aluminum ion batteries. Energy Environ Sci 5:9743–9746